

Competition between lattice distortion and charge dynamics for the charge carriers of double-layered manganites

J.-H. Park

National Synchrotron Light Source, Brookhaven National Laboratory, Upton, New York 11973-5000

T. Kimura

Joint Research Center for Atom Technology (JRCAT), Tsukuba, Ibaraki 305, Japan

Y. Tokura

Department of Applied Physics, University of Tokyo, Tokyo 113, Japan

(Received 7 August 1998)

We have investigated the characteristics of the charge carriers of the double-layered manganites, $\text{La}_{2-2x}\text{Sr}_{1+2x}\text{Mn}_2\text{O}_7$ ($x=0.35, 0.40$), using polarized O 1s x-ray absorption spectroscopy. When the system undergoes the insulator to metal transition, the spectral weight is transferred to the absorption threshold, analogous to the Drude weight in optical absorption. The charge carriers in the metallic phase contain comparable amounts of in-plane and out-of-plane character. This result is due to the competition between the tetragonal lattice distortion and the charge dynamics that force the charge carriers out of and in the plane, respectively. [S0163-1829(98)51844-9]

With the recent success of synthesis, double-layered manganites, $\text{La}_{2-2x}\text{Sr}_{1+2x}\text{Mn}_2\text{O}_7$, have attracted much attention scientifically and technologically due to their exotic electrical and magnetic properties.¹⁻³ Similar to the doped manganese perovskites,^{4,5} the system undergoes a paramagnetic insulator (PI) to ferromagnetic metal (FM) transition upon cooling through the Curie temperature (T_C) and exhibits a large negative magnetoresistance around T_C .^{1,3} Structurally, the material consists of intrinsic atomic scale magnetic multilayer tunnel junctions: each ferromagnetic metallic MnO_2 bilayer sheet is separated by a nonmagnetic insulating $(\text{La,Sr})_2\text{O}_2$ layer (I), i.e., a virtually infinite array of FM/I/FM junctions. Hence, the characteristics of the charge carriers is expected to be directly related to the electrical and magnetic properties. The charge carriers are the result of the charge dynamics of electron hopping. Thus, in most low-dimensional systems [quasi-two-dimensional (2D)/1D systems], the carriers are expected to lie mainly in the dynamic layers/chains, which are crystallographically formed. However, in the transition-metal oxides (TMO's) which are known to be strongly correlated systems, the orbital energy splitting induced by the lattice distortion can also strongly affect the characteristics of the charge carriers. In this aspect, the layered manganites may provide some insight on how the local lattice distortion competes with the charge dynamics for the charge carriers.

The metal sites in most TMO systems have octahedral site symmetry (O_h), in which each TM ion is surrounded by six oxygen ions, MO_6 , and the TM 3d orbital splits into triplet t_{2g} and doublet e_g orbitals. In the layered systems, the site symmetry of the TM ion becomes tetragonal (D_{4h}) due to the lattice distortion with the elongation of the out-of-plane M-O bonding lengths and the shortening of the in-plane M-O ones.⁶ Then the e_g orbital energy splits so that the x^2-y^2 in-plane orbital energy is separated from the $3z^2-r^2$ out-of-

plane one as schematically described in Fig. 1 [here the energy difference $\Delta \equiv \varepsilon(3z^2-r^2) - \varepsilon(x^2-y^2)$ is positive].

In high T_C cuprate systems, the parent compound contains Cu^{2+} (d^9), which has the 3d orbital full except for one x^2-y^2 state. Then the doped hole is expected to go into the $3z^2-r^2$ state due to Hund's rule. However, both the lattice distortion and the charge dynamics cooperatively force the charge carriers to lie in the CuO_2 plane. The hole takes the opposite spin x^2-y^2 state lying in the dynamic CuO_2 plane resulting in the singlet ground state, the so-called Zhang-Rice singlet state.⁷ Δ , induced by the lattice distortion, is effectively large enough to overcome the Hund's rule exchange energy, and the reduction of the in-plane Cu-O bond length enhances the in-plane hopping energy thus stabilizing the singlet ground state.⁸ Indeed, in the cuprates, the charge carriers were reported to have mostly in-plane character.⁹ Similar arguments can also be applied to the layered and chained nickelates.^{10,11}

The situation is completely different in the manganites. The ionic state of the parent manganese is Mn^{3+} (d^4) which

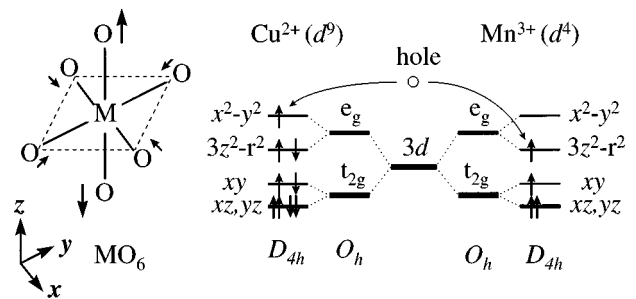


FIG. 1. Schematic diagrams of the tetragonal distortion of MO_6 octahedron and the 3d orbital energy splitting by the octahedral (O_h) and the tetragonal (D_{4h}) site symmetries. The occupations are presented for the Cu^{2+} ($3d^9$) and Mn^{3+} ($3d^4$) ions under the D_{4h} symmetry.

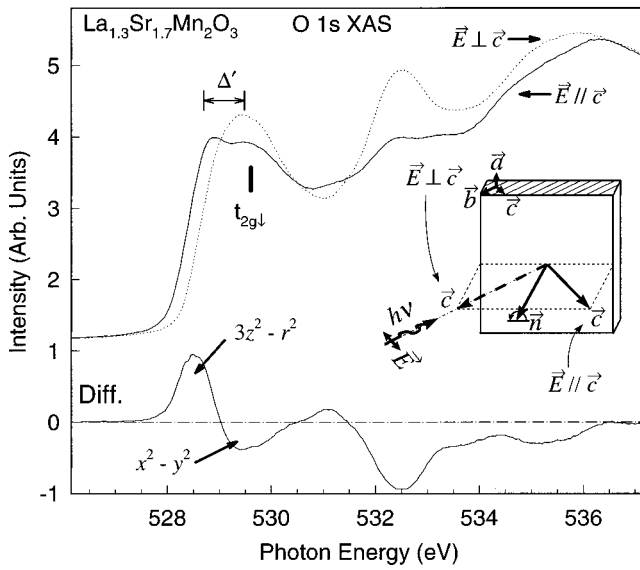


FIG. 2. O 1s XAS spectra of $\text{La}_{1.2}\text{Sr}_{1.8}\text{Mn}_2\text{O}_7$ for $\mathbf{E}||\mathbf{c}$ and $\mathbf{E}\perp\mathbf{c}$ polarization geometries represented in the figure and the difference of the spectra.

has the same spin $t_{2g}^3 e_g^1$ configuration due to Hund's rule. Here the e_g occupation stays in the out-of-plane e_g orbital ($3z^2 - r^2$), which is energetically lowered by the tetragonal distortion. Thus the doped hole can only go into the out-of-plane $3z^2 - r^2$ state. The lattice distortion forces the charge carriers out of the plane opposite to the charge dynamics, and the characteristics of the charge carriers are determined by the competition between the lattice distortion and the charge dynamics.

High-quality $\text{La}_{2-2x}\text{Sr}_{1+2x}\text{Mn}_2\text{O}_7$ ($x=0.35, 0.40$) single crystals were grown by the floating-zone method.¹² The FM-PI transition was observed in resistivity and magnetization measurements at $T_C \approx 130$ K for $x=0.35$ and $T_C \approx 120$ K for $x=0.40$. Both the in-plane and interplane resistivity exhibit large drops around T_C upon cooling. The x-ray absorption spectroscopy (XAS) measurements were performed at the renewed U4B beamline at the National Synchrotron Light Source at Brookhaven National Laboratory. The incoming photon was set to have $\sim 97\%$ linear polarization and ~ 0.2 -eV resolution. Bulk-sensitive (~ 2000 -Å probing depth) fluorescence yield spectra were recorded using a high-sensitivity seven element germanium array detector, and the spectra obtained were normalized by the photon flux. The characterization of the charge carriers using the polarized XAS requires very careful preparation of the samples and the experimental settings. (1) The samples were prepared to have the surface normal tilted $45^\circ \pm 3^\circ$ from both the c axis and the ab plane. Only with this orientation can the azimuthal rotation method, as shown in Fig. 2, provide the different polarization geometries without any optical path variations, which could contribute experimental artifacts. (2) The uncertainty in the photon energy was minimized by simultaneously recording the O 1s XAS spectrum of NiO, as a reference, which shows a sharp isolated single peak at 531.7-eV photon energy.¹² This uncertainty is expected to be less than 10 meV.

Figure 2 shows O 1s XAS spectra of $\text{La}_{2-2x}\text{Sr}_{1+2x}\text{Mn}_2\text{O}_7$ ($x=0.35$) for two different polarization

geometries, i.e., $\mathbf{E}||\mathbf{c}$ and $\mathbf{E}\perp\mathbf{c}$, and the difference of the two spectra. The overall line shapes are quite similar to those of the spectra obtained from total electron yield.¹³ The normalized absorption coefficient at an energy greater than 580 eV, well above the absorption threshold, was the same within 0.5% for the different geometries. The absorption is associated with the O $1s \rightarrow 2p$ dipole transition. In the O^{2-} ion, the $2p$ orbital is full but strong hybridization with the unoccupied Mn, $3d/4s$, La $5d/4f$, and Sr $3d/4s$ states induces O $2p$ holes. Thus the spectra reflect the unoccupied conduction band that consists of states with Mn $3d/4s$, La $5d/4f$, and Sr $3d/4s$ character. The most interest lies in the spectra near the absorption threshold, and the spectra covering the first 3 eV (528–531 eV) above threshold represent the Mn $3d$ conduction-band states that come mainly from the Mn⁴⁺ sites. As can be seen in the figure, the spectra in this region show a double-peak feature in $\mathbf{E}||\mathbf{c}$ geometry compared with a single-peak feature in $\mathbf{E}\perp\mathbf{c}$ geometry. Due to the dipole selection rules, the absorption coefficients in $\mathbf{E}||\mathbf{c}$ and $\mathbf{E}\perp\mathbf{c}$ geometries reflect the O $2p_z$ (out-of-plane) and O $2p_{x,y}$ (in-plane) character hole states, respectively. The O $2p_z/2p_{x,y}$ holes are mostly due to hybridization with the Mn $3d e_g$ -orbital, $3z^2 - r^2/x^2 - y^2$, and t_{2g} -orbital states. Therefore, the double-peak feature corresponds to the O $2p_z$ holes resulting from hybridization with the $3z^2 - r^2$ and t_{2g} unoccupied state at the low and high energies, respectively, while the single-peak feature is the O $2p_{x,y}$ holes caused by hybridization with $x^2 - y^2$ and t_{2g} unoccupied states, which are energetically close to each other. Due to the absorption energy difference Δ' for the $3z^2 - r^2$ and $x^2 - y^2$ character states, the difference spectrum in the region exhibits a peak and a dip that correspond to the $3z^2 - r^2$ and the $x^2 - y^2$ character states, respectively.¹³

One may consider the energy difference Δ' to be the orbital energy difference Δ . However, the absorption energy corresponds to the sum of the core-hole energy and the orbital state energy.¹⁴ Due to the selection rule, the O 1s core holes for the different absorption states are located at different oxygen sites. For the $2p_{x,y}$ ($x^2 - y^2$) and $2p_z$ ($3z^2 - r^2$) states, the holes are at the oxygen sites in and out of the MnO_2 plane, respectively. Because of the different chemical environments, the core-hole energy is expected to be different for the different oxygen sites, i.e., $\Delta = \Delta' - \delta$, where δ is the core-hole energy difference at the in- and out-of-plane oxygen sites. In the previous studies of the high T_C cuprates, δ was observed to be 0.3–0.5 eV.⁹ For the manganites, we also obtained $\delta = 0.4 \pm 0.1$ eV as described below, and thus the orbital energy difference Δ in the manganite is determined to be 0.4 ± 0.2 eV, which is much smaller than $\Delta \sim 2$ eV expected in the cuprates.⁸ Such a large reduction in Δ can be attributed to the *competitive* action of the lattice distortion and the charge dynamics in the manganites, opposite to the *cooperative* action in the cuprates. Indeed, the tetragonal distortion of the MnO_6 octahedron is much smaller than that of CuO_6 in the cuprates; in the manganites,^{3,15} the in-plane bond length is shorter than the out-of-plane one only by a few percent, which is much smaller than the $\sim 20\%$ difference in the cuprates.¹⁶

In order to study the charge carriers in the metallic phase, we have performed temperature dependent O 1s XAS mea-

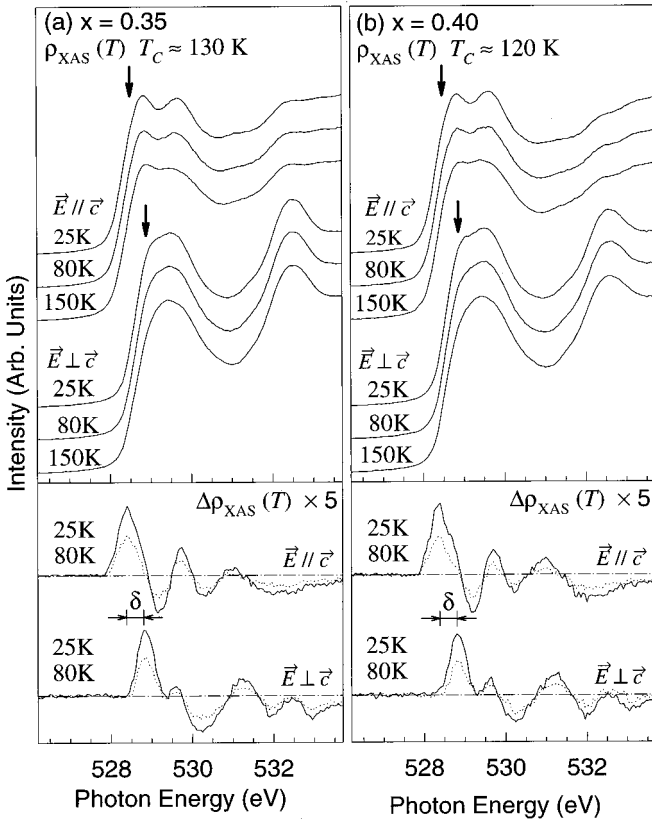


FIG. 3. Temperature-dependent O $1s$ XAS spectra [$\rho_{XAS}(T)$] for $\mathbf{E} \parallel \mathbf{c}$ and $\mathbf{E} \perp \mathbf{c}$ of $\text{La}_{2-2x}\text{Sr}_{1+2x}\text{Mn}_2\text{O}_7$; (a) $x=0.35$ and (b) $x=0.40$. The bottom panels show the corresponding spectral variations, $\Delta\rho_{XAS}(T) = \rho_{XAS}(T) - \rho_{XAS}(150 \text{ K})$, with temperature as described in the text.

measurements through T_C . Figure 3 shows the O $1s$ near-edge XAS spectra of (a) $\text{La}_{1.3}\text{Sr}_{1.7}\text{Mn}_2\text{O}_7$ ($x=0.35$) and (b) $\text{La}_{1.2}\text{Sr}_{1.8}\text{Mn}_2\text{O}_7$ ($x=0.40$) taken at three different temperatures for $\mathbf{E} \parallel \mathbf{c}$ and $\mathbf{E} \perp \mathbf{c}$. The results are basically the same for both samples. The overall line shape of the spectra are nearly identical for the different temperatures except for small variations near the absorption threshold. In the insulating phase, the density of states (DOS) is zero at the Fermi level (E_F), the insulating gap feature, but when the system undergoes the insulator to metal (I-M) transition upon cooling, the DOS changes and builds up at E_F . Thus the DOS change in the conduction band appears in the O $1s$ XAS spectrum and the spectral weight is transferred to the absorption threshold, analogous to the Drude weight in optical conductivity measurements. This spectral weight transfer is observed for both $\mathbf{E} \parallel \mathbf{c}$ and $\mathbf{E} \perp \mathbf{c}$.

The spectral variations are represented by the difference spectra, $\Delta\rho_{XAS}(T) = \rho_{XAS}(T) - \rho_{XAS}(150 \text{ K})$, shown in the bottom panels in Fig. 3. For both $\mathbf{E} \parallel \mathbf{c}$ and $\mathbf{E} \perp \mathbf{c}$, the variation increases with cooling from $T=80 \text{ K}$ to 25 K without significant change in the line shape. As can be seen in the figure, $\Delta\rho_{XAS}$ exhibits a peak at the threshold and the peak intensity increases with further cooling. These results indicate that DOS (E_F) builds up upon cooling through the I-M transition and then increases with further cooling, as observed in the doped manganese perovskites.^{17,18} The peak has an $\sim 0.7\text{-eV}$ width, which is very similar to the expected O $1s$ core-hole lifetime broadening seen in most transition-

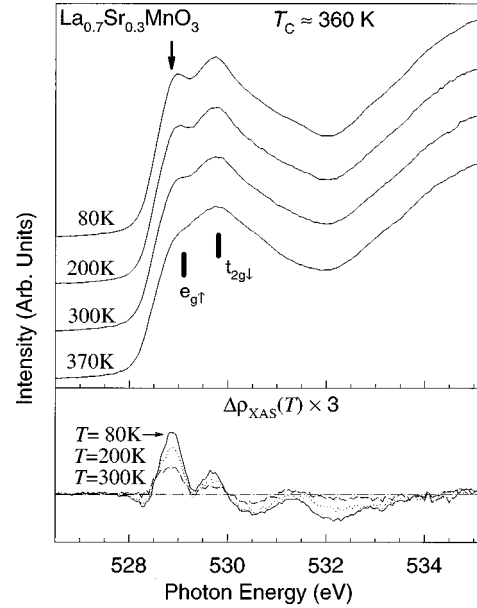


FIG. 4. Temperature-dependent O $1s$ XAS spectra [$\rho_{XAS}(T)$] and the spectral variations, $\Delta\rho_{XAS}(T) = \rho_{XAS}(T) - \rho_{XAS}(370 \text{ K})$, of $\text{La}_{0.7}\text{Sr}_{0.3}\text{MnO}_3$. A small dip appearing at $\sim 528.3 \text{ eV}$ in $\Delta\rho_{XAS}(80 \text{ K})$ and $\Delta\rho_{XAS}(200 \text{ K})$ is due to the considerably smaller phonon broadening at 80 and 200 K relative to that at 370 K.

metal oxides. The peak position is different by $\delta = 0.4 \pm 0.1 \text{ eV}$ for the different geometries since the O $1s$ core-hole energy of the out-of-plane oxygen site is smaller than that of the in-plane oxygen site due to the different chemical environments as discussed above. The peak intensity ratios of the out-of-plane ($\mathbf{E} \parallel \mathbf{c}$) O $2p_z$ to the in-plane ($\mathbf{E} \perp \mathbf{c}$) O $2p_{x,y}$ are estimated to be $53 \pm 5\%$ to $47 \pm 5\%$ for the $x=0.35$ sample and $55 \pm 5\%$ to $45 \pm 5\%$ for the $x=0.40$ sample,¹⁹ indicating that the charge carriers have similar amounts of in-plane and out-of-plane character. $\Delta\rho_{XAS}$ for the $\mathbf{E} \parallel \mathbf{c}$ shows a relatively large dip at an energy slightly above the threshold peak in comparison with that for the $\mathbf{E} \perp \mathbf{c}$. This may indicate a large reduction of the spectral weight from the $2p_z(3z^2 - r^2)$ states than the $2p_{x,y}(x^2 - y^2)$ states through the insulator to metal transition. These results indicate that not only the in-plane but also the out-of-plane physical quantities are important for the physical properties of the manganites. In recent photoemission studies,²⁰ which are very surface sensitive, the spectra exhibit only a gap feature, almost no spectral weight at E_F , rather than the metallic Fermi cutoff even in the metallic phase. At the surface, the out-of-plane interaction is disrupted, and DOS (E_F) is expected to be suppressed considerably.

Estimating the absolute value for charge carriers or the DOS (E_F) using the threshold peak intensity is impossible at the present time. However, one can compare the peak intensity with that of manganese perovskites, which are rather well studied. Figure 4 shows the temperature-dependent O $1s$ XAS spectra of a $\text{La}_{0.7}\text{Sr}_{0.3}\text{MnO}_3$ single crystal with $T_C \approx 360 \text{ K}$. The overall line shape is similar to that of the double-layered manganites. The spectra reflect the O $2p$ hole induced by the strong hybridization with the unoccupied Mn $3d/4s$, La $5d/4f$, and Sr $3d/4s$ states, and the region of the first 3 eV above the absorption threshold again comes mainly

from the Mn $3d e_g$ and t_{2g} unoccupied states of the Mn⁴⁺ sites.¹⁷ Here the energy splitting of the x^2-y^2 and $3z^2-r^2$ orbitals does not appear since the system is cubic and the local tetragonal Jahn-Teller distortion is expected to affect only the Mn³⁺ sites, but not the Mn⁴⁺ sites.²¹ The O $1s$ near-edge XAS spectra clearly show the spectral variation upon cooling through T_C , and the variation increases with further cooling. The difference spectra, $\Delta\rho_{\text{XAS}}(T) = \rho_{\text{XAS}}(T) - \rho_{\text{XAS}}(370 \text{ K})$, shown in the bottom panel of the figure, also exhibits the absorption threshold peak induced by the spectral weight transfer associated with the growing of the DOS at E_F . The overall line shape of $\Delta\rho_{\text{XAS}}(T)$ generally agrees with that for the double-layered manganites. The threshold peak intensity in $\Delta\rho_{\text{XAS}}$ (80 K) of $\text{La}_{0.7}\text{Sr}_{0.3}\text{MnO}_3$ is observed to be about 1.5 times larger than that in $\Delta\rho_{\text{XAS}}$ (25 K) of $\text{La}_{1.3}\text{Sr}_{1.7}\text{Mn}_2\text{O}_7$, indicating that DOS at E_F is somewhat smaller in the latter system. Here $T=80 \text{ K}$ in the

cubic manganite is a similar T/T_C value with $T=25 \text{ K}$ in the double-layered manganite, and the relative peak intensity was estimated per Mn.²²

In summary, we have investigated the characteristics of the charge carriers of the double-layered manganites, $\text{La}_{2-2x}\text{Sr}_{1+2x}\text{Mn}_2\text{O}_7$ ($x=0.35, 0.40$). Despite the characteristics of the layered structure, the charge carriers have comparable amounts of in-plane and out-of-plane character for both systems, resulting from the competition between the local lattice distortion and the charge dynamics, which forces the charge carriers out of and in the plane, respectively.

We thank J. B. Hastings, S. L. Hulbert, and D. S. Dessau for helpful discussions. NSLS is supported by the U.S. Department of Energy under Contract No. DE-AC02-76CH00016, and the work at UT and JRCAT was supported in part by NEDO and under a joint research agreement between NAIR and ATP.

¹Y. Moritomo, A. Asamitsu, H. Kuwahara, and Y. Tokura, *Nature* (London) **380**, 141 (1996).

²T. Kimura *et al.*, *Science* **274**, 1698 (1996).

³J. F. Mitchell *et al.*, *Phys. Rev. B* **55**, 63 (1997).

⁴G. H. Jonker and J. H. Van Santen, *Physica* (Amsterdam) **16**, 337 (1950); P. E. Schiffer *et al.*, *Phys. Rev. Lett.* **75**, 3336 (1995).

⁵C. W. Searle and S. T. Wang, *Can. J. Phys.* **47**, 2703 (1969); S. Jin *et al.*, *Science* **264**, 413 (1994).

⁶S. Sugano, Y. Tanabe, and H. Kamimura, *Multiplets of Transition Metal Ions in Crystals* (Academic, New York, 1970).

⁷F. C. Zhang and T. M. Rice, *Phys. Rev. B* **37**, 3759 (1988).

⁸G. A. Sawatzky, in *Earlier and Recent Aspects of Superconductivity*, edited by J. G. Bednorz and K. A. Müller (Springer 90, Berlin, 1989), p. 345.

⁹C. T. Chen *et al.*, *Phys. Rev. Lett.* **68**, 2543 (1992).

¹⁰E. Pellegrin *et al.*, *Phys. Rev. B* **53**, 10 667 (1996).

¹¹J. F. Ditusa *et al.*, *Phys. Rev. Lett.* **73**, 1857 (1994).

¹²S. Nakai *et al.*, *Phys. Rev. B* **36**, 9241 (1987).

¹³C.-H. Park *et al.* (unpublished).

¹⁴The absorption energy is corrected from the sum by the electron-hole pair excitonic energy ($\sim 0.2 \text{ eV}$).

¹⁵D. N. Argyriou *et al.*, *Phys. Rev. B* **55**, R11 965 (1997).

¹⁶B. Grande, H. Müller-Buschbaum, and M. Schweizer, *Z. Anorg. Allg. Chem.* **428**, 120 (1977); C. C. Torardi *et al.*, *Phys. Rev. B* **38**, 225 (1988).

¹⁷J.-H. Park *et al.*, *Phys. Rev. Lett.* **76**, 4215 (1996).

¹⁸D. D. Sarma *et al.*, *Phys. Rev. B* **53**, 6873 (1996).

¹⁹The ratios were obtained to be 52% to 48% and 54% to 46% at the first temperature cycle, and 54% to 46% and 56% to 44% at the second temperature cycle for the $x=0.35$ and 0.40 samples, respectively.

²⁰D. S. Dessau *et al.*, *Phys. Rev. Lett.* **81**, 192 (1998); R. Liu *et al.* (private communication).

²¹A. J. Millis, B. I. Shraiman, and R. Mueller, *Phys. Rev. Lett.* **77**, 175 (1996).

²²The O $1s$ absorption intensity well above the edge corresponds to the O $1s$ photoionization cross section, and the difference in the number of oxygen ions per the manganese ion was taken into account.